Geophysical Research Letters

RESEARCH LETTER
10.1029/2024GL112516

Increasing the Glen–Nye Power-Law Exponent Accelerates Ice-Loss Projections for the Amundsen Sea Embayment, West Antarctica

Benjamin Getraer[1] **and Mathieu Morlighem**[1]

[1]Department of Earth Sciences, Dartmouth College, Hanover, NH, USA

Key Points:

- Increasing Glen–Nye exponent from $n = 3$ to 4 leads to 32 ± 14% greater Amundsen Sea Embayment ice loss by 2100, 70 ± 15% by 2300 in our model
- Uncertainty in ice loss due to n is comparable to uncertainty from different high-emission (RCP8.5) climate forcings by 2100
- Regions most sensitive to n are located where changes in strain rates are largest, such as close to the grounding line and shear margins

Supporting Information:

Supporting Information may be found in the online version of this article.

Correspondence to:

B. Getraer,
benjamin.p.getraer.gr@dartmouth.edu

Citation:

Getraer, B., & Morlighem, M. (2025). Increasing the Glen–Nye power-law exponent accelerates ice-loss projections for the Amundsen Sea Embayment, West Antarctica. *Geophysical Research Letters*, *52*, e2024GL112516. https://doi.org/10.1029/2024GL112516

Received 13 SEP 2024
Accepted 27 FEB 2025

Abstract Glacier flow is typically modeled using a power-law rheology known as the Glen–Nye flow law, with the power n assumed to be 3. However, recent research and past observations suggest that $n = 4$ may better represent ice flow in some locations. We lack a quantitative understanding of how much n affects ice-loss projections, and its significance relative to other sources of uncertainty. Here, we test the effect of $n = 3$ versus $n = 4$ in a series of 300-year forward simulations of the Amundsen Sea Embayment, West Antarctica. We find that in periods of rapid grounding line retreat, uncertainty in n leads to a larger spread in ice-loss projections than the spread due to uncertainty in climate forcing. The spatial sensitivity of n is generally proportional to change in strain rates, so we expect regions undergoing more moderate dynamic change to be less sensitive to n.

Plain Language Summary Our understanding of future sea level rise due to shrinking ice sheets is informed by mathematical representations of the movement of glaciers, in addition to melting and accumulation of ice. Fundamental to this mathematical theory is the Glen–Nye flow law, which describes solid ice as a viscous fluid that flows exponentially more easily under greater force. The numerical parameters of this equation are difficult to estimate, and most studies assume that the exponent n—which has the greatest impact on ice flow—is always equal to 3. Recent research suggests that a value of 4 better represents the actual behavior of glaciers in some places. We set out to answer whether this difference in n significantly affects mathematical simulations of glaciers enough that it should be considered in estimates of future sea level rise. We find that $n = 4$ does make a significant difference in the fastest retreating sector of the Antarctic Ice Sheet, because the ice is able to change much faster. Beyond the 21st century, the value of n in this region is at least as important to estimates of ice loss as the trajectory of future melt and snowfall patterns.

1. Introduction

Our understanding of future sea level rise due to shrinking ice sheets is informed by mathematical representations of ice flow (e.g., Goelzer et al., 2020; Seroussi et al., 2020), and assumptions about ice-flow properties within these models may bias our expectations for future change. Here, we quantify the effect of such an assumption on a critical region of ice-sheet change, the Amundsen Sea Embayment (ASE), West Antarctica.

The Glen–Nye flow law is a simple, ubiquitous model for the deformation of glacial ice and is fundamental to the equations which govern ice flow. This equation describes the relation of deviatoric stress to strain rate, treating ice as a non-Newtonian, isotropic, viscous fluid defined by a power law:

$$\dot{\varepsilon}_e = A\tau_e^n \tag{1}$$

where $\dot{\varepsilon}_e$ (s^{-1}) is effective strain rate, τ_e (Pa) is effective deviatoric stress, A $(\mathrm{Pa}^{-n}\ \mathrm{s}^{-1})$ is the rate factor, and n is the dimensionless power-law exponent (Glen, 1952; Nye, 1953). Nye (1957) extended this relationship to multiaxial states of stress by writing this law in tensorial form:

$$\boldsymbol{\tau} = 2\mu\dot{\boldsymbol{\varepsilon}} \tag{2}$$

where $\boldsymbol{\tau}$ is the deviatoric stress tensor, $\dot{\boldsymbol{\varepsilon}}$ is the strain rate tensor, and μ (Pa s) is ice viscosity defined as:

$$\mu = \frac{B}{2\,\dot{\varepsilon}_e^{\frac{n-1}{n}}}. \quad (3)$$

with $B = A^{-1/n}\ \left(\text{Pa s}^{1/n}\right)$ being an alternative formulation of the rate factor, which we will use going forward.

The exponent n fundamentally alters the ice-flow behavior predicted by the Glen–Nye flow law. A value of $n = 1$ treats ice as a Newtonian fluid (viscosity is insensitive to changes in stress), and results in linear equations that become simple to solve. Higher values of n introduce a shear-thinning behavior, with a non-linear sensitivity of strain rate to changes in stress. A higher exponent therefore results in faster response in regions undergoing dynamic change, and greater numerical complexity due to the non-linear system of equations.

Since the introduction of the Glen–Nye flow law in the 1950s, efforts to determine an appropriate value for n have included laboratory experiments, direct field measurements, and remote-sensing data, combined with deformation-model analysis (Cuffey & Paterson, 2010; Weertman, 1983). While a range of values from 2 to 4 have been found, $n \approx 3$ has generally been interpreted as most consistent with field observations (Cuffey & Paterson, 2010; Weertman, 1983). Accordingly, the baseline assumption in most ice-sheet-model verification and implementation has been to simply set $n = 3$ uniformly everywhere (e.g., Cornford et al., 2020; Pattyn et al., 2008).

The assumption of $n = 3$ for ice deformation is not universally supported. Experimental studies have found that n is stress dependent, with n generally increasing at higher stresses, reflecting shifts in the mechanisms of creep which accommodate ice deformation at the grain scale (Goldsby & Kohlstedt, 2001; Montagnat & Duval, 2004). Theoretical frameworks allowing for the interaction of multiple stress-dependent creep mechanisms and feedback with grain-size evolution suggest that n may still have a relatively stable value across a wide range of realistic stress conditions, with n typically being around 3 (Behn et al., 2021) or 4 (Ranganathan & Minchew, 2024), depending on the assumptions made about grain-size evolution. Experimental work supports $n \approx 4$ for flowing ice with varying grain size and microstructure (Qi et al., 2017).

Additionally, values of $n > 3$ have been inferred from real-world glaciers. Careful stress analysis of borehole tilts in Athabasca Glacier, Canada, found a best fit of $n \approx 3.6$–4.3 (Paterson & Savage, 1963; Raymond, 1973). Thomas et al. (1980) found that the dynamics and geometry of the Roosevelt Island ice dome, Antarctica, were consistent with values of $n \approx 3.7$–4.2. A value of $n = 4$ for Roosevelt Island was corroborated by a numerical thermomechanical simulation reproducing measured radar stratigraphy (Martín et al., 2006). Cuffey and Kavanaugh (2011) used a probabilistic reanalysis with a numerical model to determine a best fit of $n = 3.5$ for Taylor Glacier in the Transantarctic Mountains. Gillet-Chaulet et al. (2011) used phase-sensitive radar to measure variation in vertical strain rates adjacent to ice divides on the Greenland Ice Sheet, finding they were best fit by $n \approx 4.5$. A regression analysis of northern Greenland Ice Sheet geometry and surface velocities using the shallow-ice approximation found a best fit for $n = 4.1$ (Bons et al., 2018). More recently, Millstein et al. (2022) examined the stress–strain rate relation over large parts of Antarctic ice shelves undergoing close-to-pure extensional flow, and found a best fit of $n = 4$. These findings suggest that, in some places, values of $n > 3$ provide the best representation of ice dynamics using the Glen–Nye flow law, and that a universal assumption of $n = 3$ could be a source of bias in numerical ice-sheet simulations.

Despite decades of work attempting to estimate appropriate values for n, the possibility that n could be greater than 3 has not received significant analysis in numerical models. One study, Zeitz et al. (2020), examined the sensitivity of flow-law parameters in a simplistic idealized ice-sheet model, suggesting that the value of n could impact dynamic response in warming ice. However, their comparisons began with different initial conditions and drove dynamic change through instantaneous warming and a temperature-dependent rate factor, making the results unsuited to interpreting uncertainty in more complex projections of sea level rise (Zeitz et al., 2020). This gap leaves fundamental questions unanswered: How much does the choice of n affect the simulated evolution of realistic glacial flow? Does a difference between $n = 3$ and $n = 4$ significantly affect near-future projections of sea-level-rise contributions from ice sheets compared to other sources of uncertainty?

We answer these questions by comparing results for $n = 3$ and $n = 4$ from a series of numerical ice-sheet experiments. We use six benchmark climate forcings for the high-emission, RCP8.5 warming scenario selected for the Ice Sheet Model Intercomparison Project for CMIP6 (ISMIP6, Nowicki et al., 2020). We choose the ASE for

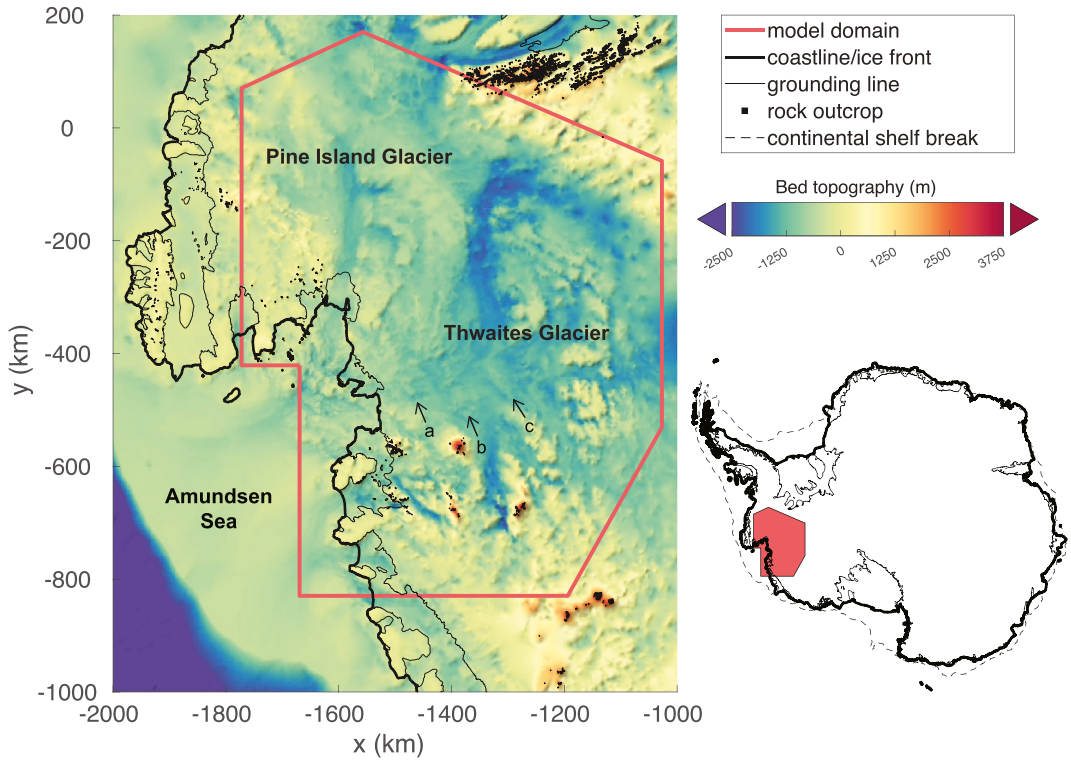

Figure 1. Bed topography of the Amundsen Sea Embayment, West Antarctica, with the extent of our numerical domain outlined in red. Subglacial ridges such as (a), (b), and (c) may mitigate the initial retreat phase of Thwaites Glacier toward deep subglacial basins (e.g., Schwans et al., 2023). Map data from Amblas (2018), Gerrish et al. (2020, 2024), and Morlighem (2022); x and y are in polar stereographic coordinates.

our experimental domain because it is the fastest changing region of ice loss in Antarctica and has the potential for large near-future contributions to sea level rise (e.g., Feldmann & Levermann, 2015; Rignot et al., 2019; Scambos et al., 2017; Seroussi et al., 2020). Ice loss from the ASE is expected to increase due to the geometry of its catchments, which are grounded on a bed that deepens inland to subglacial basins far below sea level, potentially triggering the marine ice sheet instability (MISI, Denton et al., 1979; Hughes et al., 1981; Pattyn & Morlighem, 2020; Schoof, 2012; Thomas, 1979; Thomas & Bentley, 1978; Weertman, 1974). The rate of future ice loss from the ASE is therefore expected to depend not only on regional mass balance, but also on the rate of dynamic thinning, which sets the pace of MISI-induced grounding line retreat. The importance of dynamic thinning in setting the rate of ice loss from basins undergoing MISI suggests that these are locations for which model projections would be particularly sensitive to the choice of n (Ranganathan & Minchew, 2024; Schoof, 2012).

2. Methods

We use the Ice-sheet and Sea-level System Model (ISSM, Larour et al., 2012) to simulate ice-flow dynamics of the ASE sector of the West Antarctic Ice Sheet using the shelfy-stream approximation equations of motion (MacAyeal, 1989). The spatial domain includes Pine Island and Thwaites glaciers and their ice shelves, as well as the Crosson and Dotson ice shelves and their tributaries (Figure 1).

We run a total of 12 different experiments. We use surface mass balance and ice-shelf melt from the six CMIP5 benchmark climate models selected for ISMIP6 ice-sheet-model forcings to represent a range of possible variability due to external climate dynamics (Barthel et al., 2020). For each ISMIP6 member, we run one experiment with $n = 3$ and one with $n = 4$, maintaining otherwise identical initial conditions.

We construct a triangular mesh, spatially refined based on initial velocity, with a nominal resolution ranging from 1 to 22 km (Figure S1 in Supporting Information S1). Bed topography and initial ice thickness are taken from

BedMachine Antarctica v3 (Morlighem, 2022; Morlighem et al., 2020). Initial ice velocities are taken from the MEaSUREs InSAR-Based Antarctica Ice Velocity Map, v2 (Mouginot et al., 2017; Rignot et al., 2017). Both of these data sets integrate observations over multiple years, and we choose a nominal start time of $t_0 = 2013$. After initialization, each experiment is run forward in time until 2300.

Sub-element grounding line migration is implemented following Seroussi et al. (2014). Ice-front position is held constant throughout the simulations, and along domain's outer boundary we impose Dirichlet conditions on ice velocity such that $\mathbf{v}(x, y, t) = \mathbf{v}(x, y, t_0)$. We use a Budd friction law (Budd et al., 1979), and calibrate the friction coefficient (over grounded ice) and rate factor B (over floating ice) using inverse modeling following Morlighem et al. (2013) (Text S1 in Supporting Information S1).

To isolate the effect of n on future projections, our models must share identical initial conditions with $n = 3$ and $n = 4$. We choose to keep initial viscosities (and therefore initial strain rates) identical for each experiment by rescaling the rate factor B for different n. We define B_{n_0} for $n_0 = 3$ and find B_n for $n = 4$, such that $\mu_n = \mu_{n_0}$:

$$B_n = B_{n_0}\, \dot{\varepsilon}_e(t_0)^{1/n_0 - 1/n} \tag{4}$$

We use linear finite-elements with constant B, and therefore constant viscosity, over each element. This initialization scheme allows us to rescale B for any n such that initial ice viscosity and velocity are identical within machine precision.

Climate forcings for surface mass balance and sub-ice-shelf basal melting come from the model ensemble and implementation selected by ISMIP6 (Nowicki et al., 2020, 2021; Seroussi et al., 2020). These climate forcings are derived from atmosphere–ocean coupled global climate models, with the model ensemble selected for ability to reproduce the observational record and for diversity of future climate projections (Barthel et al., 2020; Nowicki et al., 2020). The six-member ensemble of target experiments for Antarctica selected by ISMIP6 and used in this study comprises CCSM4, MIROC-ESM-CHEM, NorESM1-M, HadGEM2-ES, CSIRO-Mk3-6-0, and IPSL-CM5A-MR (Barthel et al., 2020). For each climate experiment we use forcings from the RCP8.5 projection to compare the spread due to differences in n to uncertainty related to different representations of the same high-emission climate scenario. For details on how ensemble members differ in their climate forcings, the reader is directed to Barthel et al. (2020) and Nowicki et al. (2020). We choose the RCP8.5 projections as they induce the strongest grounding line change, and therefore set an approximate upper bound on the sensitivity of mass loss to n within our model framework.

Climate forcings are provided every year until 2100, beyond which the standard ISMIP6 model forcing does not extend. In our experiments, we hold the 2100 climate forcings constant for all later time steps. For details on ISMIP6 climate-forcing protocols, see Jourdain et al. (2020). The experiments conducted here have analogous setup to `exp05`, `exp06`, `exp08`, `expA5`, `expA6`, and `expA7` from Seroussi et al. (2020) (see their Table 1).

To analyze the outcomes of each experiment, we compare changes in total mass above flotation, M (kg), which is transformed to sea level equivalence, SLE (m), by dividing by the density of freshwater $\left(\rho_w = 1000 \text{ kg m}^{-3}\right)$ and surface area of the ocean $\left(S_o = 3.618 \times 10^{14} \text{ m}^2\right)$. Two measures are chosen to compare the spread in M for each experiment set: To measure the spread of experiments due to climate forcing, we look at the range and standard deviation of the $n = 3$ and $n = 4$ experiments, respectively; To measure the spread of experiments due to choice of n, we look at the maximum and the mean of the difference between each $n = 4$ and $n = 3$ experiment pair.

Additionally, to investigate the spatial sensitivity of future projections to n, we calculate the sensitivity of total volume above flotation, V $\left(\text{m}^3\right)$, with respect to n using automatic differentiation following Morlighem et al. (2021). This approach provides the gradient of the final volume above flotation, $\mathcal{D}V(n_0)$ (m), to a reference n_0 at any point in the model domain at the spatial resolution of the mesh (see Text S1 in Supporting Information S1).

The sensitivity of the total final mass above flotation, M, with respect to n is $\mathcal{D}M(n_0) = \rho\, \mathcal{D}V(n_0)$ $\left(\text{kg m}^{-2}\right)$, where ρ is the density of glacial ice $\left(917 \text{ kg m}^{-3}\right)$. In our automatic differentiation analysis, the gradient $\mathcal{D}V(n_0)$ is calculated for $n_0 = 3$, with CCSM4 climate forcings. Sensitivities are defined for a specific time t, and we choose 15 years into our model run to capture emergent sensitivity patterns with a minimum of complexity

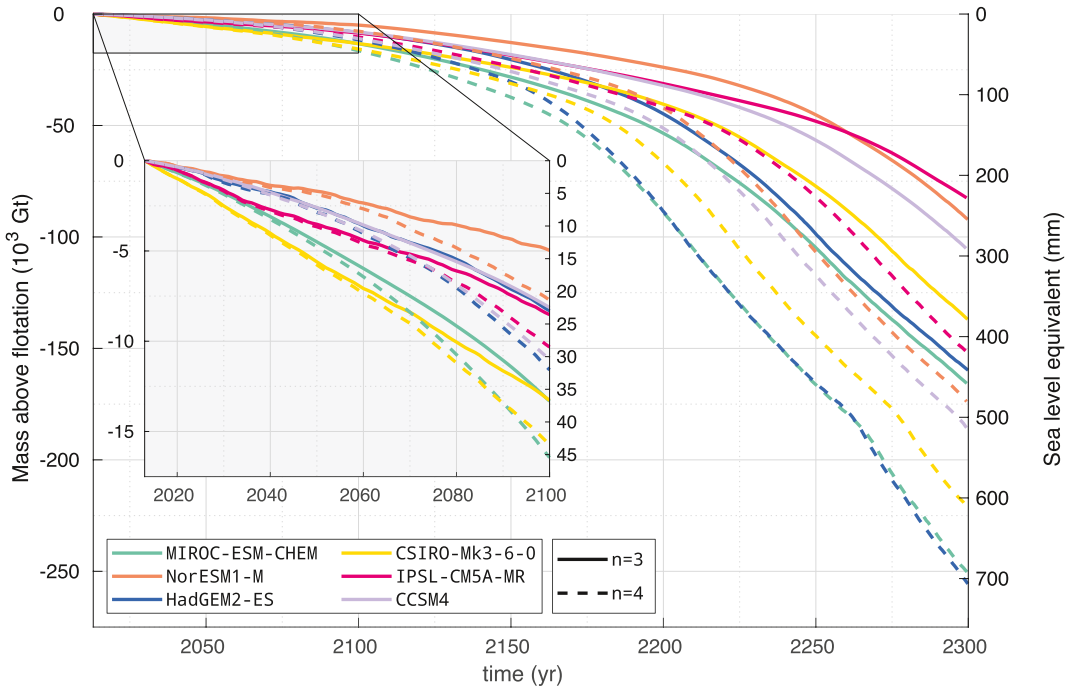

Figure 2. Change in total mass above flotation for the Amundsen Sea Embayment, 2013–2300, for all 12 experiments: six ISMIP6 RCP8.5 climate forcings (unique colors), and two power-law exponents ($n = 3$, solid line; $n = 4$, dashed line). Inset: same results, expanded for 2013–2100.

introduced by the cumulative influence of grounding line retreat. Choosing a later t does not change the overall sensitivity results.

3. Results

For all six ISMIP6 climate forcings, $n = 4$ experiments produce faster ice loss than their respective $n = 3$ experiment (Figure 2). The rate of M change is roughly linear in the first phase of grounding line retreat, and then transitions to a much steeper rate of mass loss in a secondary, accelerated retreat phase. Overall, the ASE domain loses $32 \pm 14\%$ more ice by 2100 with $n = 4$ than with $n = 3$, increasing with time to about $70 \pm 15\%$ more ice by 2300.

The first phase of retreat is characterized by a rapid linear divergence between experiments due to different climate forcings (Figure 3, red and blue lines), and initially slower but accelerating divergence between the $n = 3$ and $n = 4$ experiments (Figure 3, black lines). The second phase of retreat is characterized by a steeper rate of mass loss depending on n, with all $n = 4$ experiments showing a similar rate of mass loss $\left(-1.69 \pm 0.30 \times 10^3 \text{ Gt yr}^{-1}\right)$, about 1.5× larger than the rate of mass loss from the $n = 3$ experiments $\left(-1.09 \pm 0.12 \times 10^3 \text{ Gt yr}^{-1}\right)$ by 2300 (Figure 2 and Figure S2 in Supporting Information S1).

The transition, from variable rates of mass loss depending on the climate scenario, to a consistent rate of mass loss controlled by n, occurs between 2200 and 2300 for experiments with $n = 3$, and between 2150 and 2250 for experiments with $n = 4$ (inflection points in Figure 2 and Figure S2 in Supporting Information S1). The $n = 4$ experiments transition to the second phase of ice loss earlier and with a higher rate of ice loss than the $n = 3$ experiments, significantly increasing the spread between the two sets, which exceeds the average spread due to different climate forcings between 2150 and 2250. By 2250, the increased mass loss observed when changing n from 3 to 4 is approximately the same magnitude as the total range in mass loss due to choice of climate forcing (Figure 3).

The maximum spread due to climate forcings (Figure 3, solid red and blue lines) tracks increasingly higher than the average spread due to climate forcings (dashed red and blue lines), demonstrating the strong and unevenly distributed divergence seen in a sample of just six climate realizations. Conversely, the maximum spread due to

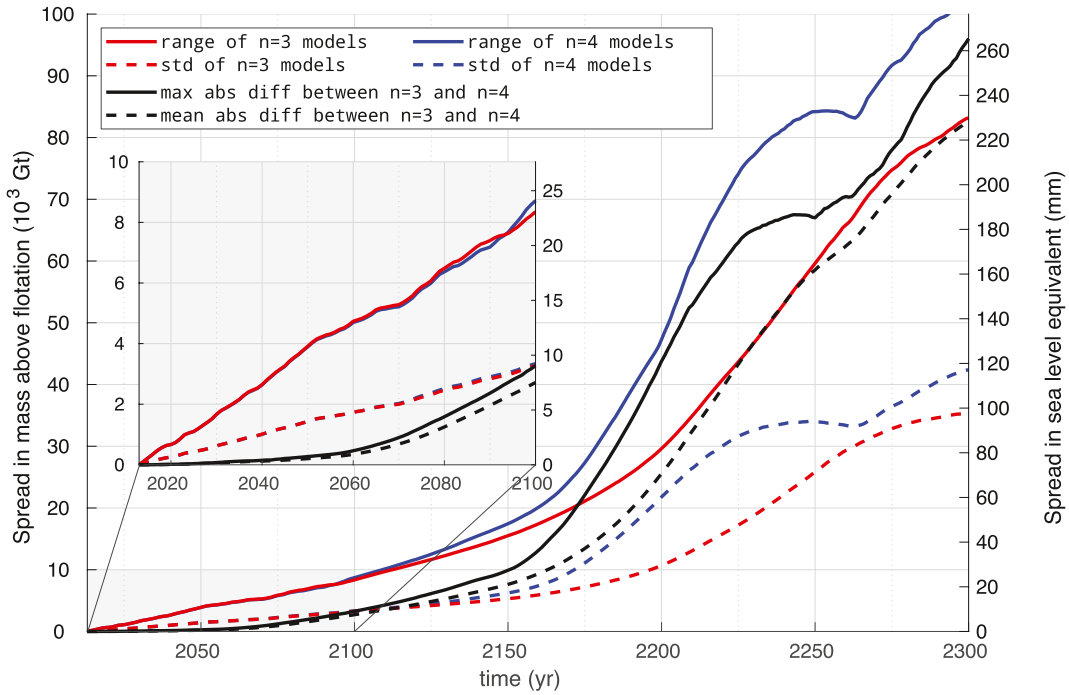

Figure 3. Comparison of climate forcings and choice in n as sources of uncertainty in the total mass above flotation for the Amundsen Sea Embayment, 2013–2300. Red: spread due to climate forcings from the six-member ISMIP6 RCP8.5 ensemble, for $n = 3$. Blue: the same, shown for the $n = 4$ experiments. Black: spread due to changing n from 3 to 4 between each climate-forcing pair. Inset: same results, expanded for 2013–2100.

changing n from 3 to 4 (solid black line) tracks more consistently with the average spread due to changing n (dashed black line), showing that changes in n have a relatively consistent effect across models with different climate forcings.

Using auto-differentiation, we find that mass loss is only significantly affected by changes to n in particular areas —the grounding zones and lower shear margins of the ice streams—and is otherwise insensitive to choice in n over the vast majority of the domain (Figure 4c). While these sensitive regions have high effective strain rates, the magnitude of the strain rate alone does not fully explain the spatial pattern or sign of the sensitivity $DM(n)$

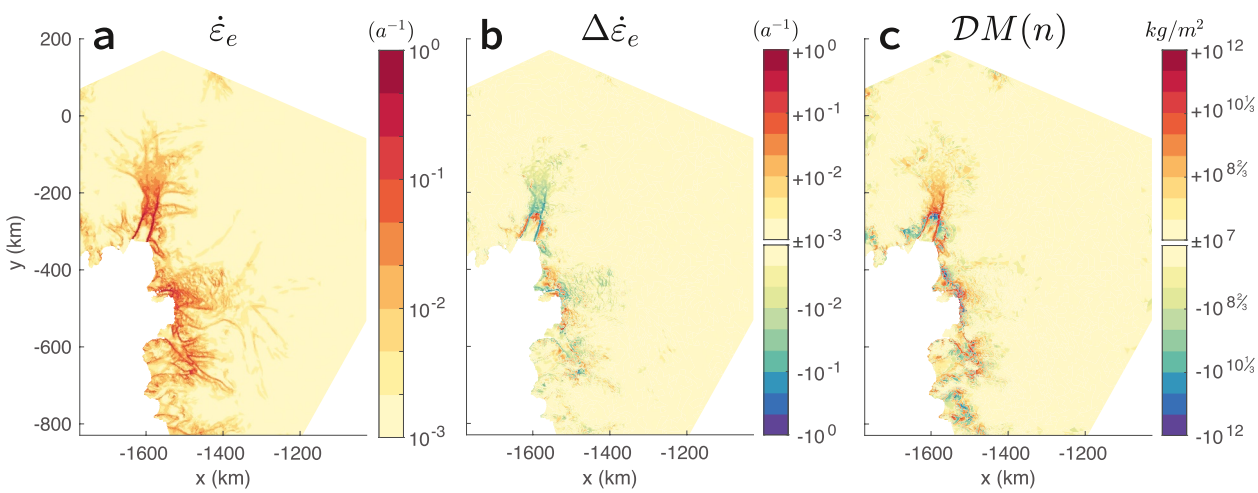

Figure 4. (a) Initial effective strain rate (from Mouginot et al. (2017) and Rignot et al. (2017)). (b) Change in effective strain rate between 2013 and 2028. (c) Sensitivity of mass above flotation with respect to n, between 2013 and 2028. Panels (b, c) show results from the CCSM4, $n = 3$ experiment. The inverse relationship between $\Delta\dot{\varepsilon}$ and $DM(n)$ reflects the relationship between $\dot{\varepsilon}$ and μ in Equation 3, showing that in regions where $\dot{\varepsilon}$ is increasing, higher n will lead to greater mass loss.

(Figure 4a). Instead, we find that $\mathcal{D}M(n)$ is generally negatively correlated with *change* in effective strain rate (Figure 4b): In regions where strain rates are increasing, an increase in n leads to more ice loss (negative sensitivity $\mathcal{D}M(n)$), while in regions where strain rates are decreasing, an increase in n leads to less ice loss (positive sensitivity $\mathcal{D}M(n)$).

4. Discussion

The two phases of ice loss observed in our results (Figure 2) reflect stages of grounding line retreat in the Thwaites Glacier basin. The initial, slower phase of mass loss reflects *ridge-to-ridge* pacing of retreat, as subglacial topography provides an ephemeral stabilizing effect (e.g., Morlighem et al., 2020; Schwans et al., 2023). After the grounding line retreats past the last of these ridges, the initial phase gives way to more-rapid ungrounding that progresses up the entirety of the Thwaites Glacier trunk into increasingly deep subglacial basins (Figure 1 and Figure S3 in Supporting Information S1).

Initial rates of ice loss in our experiments are controlled predominantly by climate forcing (Figure 2, inset). The spread of mass-loss projections within the first few decades reflects the influence of different climate forcings between experiments, while the effect of changing n is comparatively marginal over that time period, as model viscosities slowly diverge from their shared initial state (Figures 2 and 3, inset). In the secondary retreat phase, convergence in the rate of mass loss across experiments for a given n suggests that dynamic thinning controlled by n dominates the effects of climate forcings (Figure 3).

In our results, the timing of ungrounding from the upstream ridges under Thwaites Glacier (the inflection point between the two phases of retreat) is a determining factor in the total amount of ice lost by a given time, and occurs ~50 years sooner for $n = 4$ compared to $n = 3$ (Figure 2 and Figure S2 in Supporting Information S1). However, the order in which climate experiments with a shared n reach this transition is identical for both $n = 3$ and $n = 4$; in other words, for a given n, climate forcing has a strong influence on when the secondary retreat phase begins. The dependence of this transition timing on climate forcing is expected: The ridge-to-ridge phase of retreat, which is ongoing, includes periods of ephemeral quasi stability where the strength of ocean melting at the grounding line has a strong effect on the retreat rate (Christie et al., 2023; Milillo et al., 2019; Schwans et al., 2023; Seroussi et al., 2017).

We interpret that the value of n is a considerable, but not dominant, source of uncertainty in projections of ASE contributions to sea level rise during the initial ridge-to-ridge phase of future Thwaites Glacier grounding line retreat. In the faster secondary retreat phase, which persists until the entire Thwaites Glacier drainage is ungrounded, we find that the value of n directly limits the rate of ice loss. In the model framework presented here, this result suggests that n is a critical consideration on time scales exceeding 100 years.

While we contextualize our results by comparing the relative timing of Thwaites Glacier retreat in our experiments, constraining the absolute timing of this retreat is not the aim of this study. Our experiments use vertically integrated ice dynamics, simplified ocean and sliding parameterizations, and no representation of subglacial hydrology, calving, or solid Earth deformation. Constraining a likely real-world timeline of retreat from the ridges on which Thwaites is currently grounded requires a more thorough understanding of grounding-line processes and more sophisticated modeling approaches in the areas described above (e.g., Bett et al., 2024; Book et al., 2022; Milillo et al., 2019; Rignot et al., 2024; Schwans et al., 2023; Summers et al., 2023).

Ice viscosity only changes from its initial value when there is a change in the strain rate (Equation 3). Therefore, ice dynamics are only sensitive to the value of n where strain rates change significantly over the time period of interest. While the potential for large change exists in ice with high initial strain rates, the magnitude of strain rate alone does not determine sensitivity to n. For example, ice loss over the first 15 years in our model is not sensitive to our choice for n in the upper shear margins of the ice streams. Despite high local strain rates, there is insufficient change in strain rates over that time interval for n to affect the viscosity (Figure 4).

Our model is most sensitive to the value of n in the grounding zones and lower shear margins of the ice streams (Figure 4c), which migrate upstream as the grounding line retreats. The migration of these critical zones into previously lower stress ice leads to increased strain rates and stresses upstream, as the dynamic shear-thinning wave ungrounds the ice sheet—which would be accompanied by a transition toward higher n based on stress-dependent, spatially variable models of n (e.g., Goldsby & Kohlstedt, 2001). Further sensitivity testing could shed light on whether a stress-dependent n model produces the same outcome as a model with a constant $n = 4$

everywhere, or if feedbacks between n and the stress field lead to sufficiently different dynamics to merit consideration.

Stress dependent models become more complicated when considering softening feedbacks, such as the development of preferred fabric orientations, grain size evolution, and shear heating, which can work against the buildup of stress by decreasing the viscosity (e.g., Behn et al., 2021; Minchew et al., 2018). Softening is typically represented in a spatially variable B, whereby a smaller B accommodates a lower viscosity without increasing n (Cuffey & Paterson, 2010). A spatially and temporally varying B could allow for smoother, more uniform stresses across sharp transitions in strain rates, which would affect the modeled evolution of critical zones. The co-dependence of stress, strain rate, B, and n make these feedbacks hard to untangle, but is important in determining the true influence of n on the evolution of real-world glacial ice.

Recent work by Ranganathan and Minchew (2024) proposes mapping B and n to temperature and stress based on empirically derived stress dependence, experimental results, real-world observations, and a theoretical model for grain size. Such a framework is an important step toward placing meaningful and self-consistent constraints on spatially and temporally evolving rheological parameters. In their work, $n \approx 4$ emerges as an essentially uniform value for all ice streams and ice shelves across Antarctica, likely precluding the possibility of dynamic feedback involving the stress dependence of n. However, replacing a uniform assumption of $n = 3$ with a uniform assumption of $n = 4$ leaves persisting inconsistencies with experimental results and other grain evolution models (e.g., Behn et al., 2021), and previous studies which inferred lower n values for some areas of Antarctic ice shelves (e.g., Jezek et al., 1985; Thomas, 1973).

While the question of what value of n is appropriate for a given region remains imperfectly understood, our results show that in fast-changing ice, n plays a significant role in pacing the rate of mass loss. At the extremes of unmitigated MISI, grounding line retreat may be limited only by dynamic thinning, at which point n is the dominant constraint on the rate of ice loss. Given our choice of model domain and warming scenario, we interpret these results as an upper bound on how much n may affect the evolution of ice dynamics within the model framework presented here. Additional experiments, not shown here, tested the same experimental framework with constant climate forcings, and found generally consistent patterns of retreat and sensitivity, with the primary differences being the timing of the retreat phases. We expect that in most locations, undergoing far slower change, the influence of n on glacier dynamics at similar temporal and spatial scales is negligible. However, regions experiencing rapid changes in their driving stresses and strain rates—where sensitivity to n is likely to be significant—are also those with consequential potential for near-future sea level rise.

Finally, $n = 4$ not only has implications for simulated ice dynamics, but also for the computational cost of running numerical simulations. Changing n from 3 to 4 makes the stress-balance equations more non-linear, and in our experiments optimized iterative solvers take longer to converge, often failing. The frequent need to use a direct numerical solver leads to a 206% increase in computational time on average when using $n = 4$ compared to $n = 3$ in our experiments.

5. Conclusion

We quantify the impact of assuming $n = 3$ on projections of ASE ice loss by conducting experiments with a numerical ice-sheet model. In our experiments, $n = 4$ leads to 32% more ice loss on average by 2100 compared to $n = 3$; a spread in model uncertainty of similar magnitude to the variance we find due to climate uncertainty, as represented by the six-member ensemble of ISMIP6 RCP8.5 climate-forcing experiments. Beyond 2100, the value of n becomes a greater source of model uncertainty than climate forcing, especially after Thwaites Glacier's grounding line retreats past the last stabilizing ridges. The value of n is most important in regions undergoing dynamic change where the viscosity is changing over relevant time scales, such as the lower shear margins and grounding zones of the ice streams. Projections for rapidly changing sectors should be interpreted as underestimates until new rheological models that account for spatio-temporal variability in n are developed and implemented in large-scale ice-sheet models.

Data Availability Statement

All data and code used in this study are publicly available. Code written for the setup of these experiments and figures here can be found maintained in a repository on GitHub at https://github.com/bgetraer/proj-n4 and archived on Zenodo at https://doi.org/10.5281/zenodo.13750794 (Getraer, 2024). The Ice-sheet and Sea-level System Model (ISSM) can be downloaded from GitHub at https://github.com/ISSMteam/ISSM (ISSM Team, 2024). MEaSUREs BedMachine Antarctica (version 3) is available from the National Snow and Ice Data Center at https://doi.org/10.5067/FPSU0V1MWUB6 (Morlighem, 2022). ISMIP6 forcing data sets are available at GHub after login/creation of an account: https://theghub.org/resources/4743 (Nowicki et al., 2021).

Acknowledgments
Thank you to Brent Minchew and an anonymous reviewer for their helpful comments as referees, which improved the clarity of this work. Thank you to Alexander Getraer for feedback on an earlier manuscript draft. This work is from the PROPHET project, a component of the International Thwaites Glacier Collaboration (ITGC). Support from National Science Foundation (NSF: Grant 1739031) and Natural Environment Research Council (NERC: Grants NE/S006745/1 and NE/S006796/1). ITGC Contribution No. ITGC-136.

References

Amblas, D. (2018). Antarctic continental shelf break (shapefile) [Dataset]. *Scott Polar Research Institute, University of Cambridge, PANGAEA*. https://doi.org/10.1594/PANGAEA.890863

Barthel, A., Agosta, C., Little, C. M., Hattermann, T., Jourdain, N. C., Goelzer, H., et al. (2020). CMIP5 model selection for ISMIP6 ice sheet model forcing: Greenland and Antarctica. *The Cryosphere*, *14*(3), 855–879. https://doi.org/10.5194/tc-14-855-2020

Behn, M. D., Goldsby, D. L., & Hirth, G. (2021). The role of grain size evolution in the rheology of ice: Implications for reconciling laboratory creep data and the glen flow law. *The Cryosphere*, *15*(9), 4589–4605. https://doi.org/10.5194/tc-15-4589-2021

Bett, D. T., Bradley, A. T., Williams, C. R., Holland, P. R., Arthern, R. J., & Goldberg, D. N. (2024). Coupled ice–ocean interactions during future retreat of West Antarctic ice streams in the Amundsen Sea sector. *The Cryosphere*, *18*(6), 2653–2675. https://doi.org/10.5194/tc-18-2653-2024

Bons, P. D., Kleiner, T., Llorens, M.-G., Prior, D. J., Sachau, T., Weikusat, I., & Jansen, D. (2018). Greenland Ice Sheet: Higher nonlinearity of ice flow significantly reduces estimated basal motion. *Geophysical Research Letters*, *45*(13), 6542–6548. https://doi.org/10.1029/2018GL078356

Book, C., Hoffman, M. J., Kachuck, S. B., Hillebrand, T. R., Price, S. F., Perego, M., & Bassis, J. N. (2022). Stabilizing effect of bedrock uplift on retreat of Thwaites Glacier, Antarctica, at centennial timescales. *Earth and Planetary Science Letters*, *597*, 117798. https://doi.org/10.1016/j.epsl.2022.117798

Budd, W. F., Keage, P. L., & Blundy, N. A. (1979). Empirical studies of ice sliding. *Journal of Glaciology*, *23*(89), 157–170. https://doi.org/10.3189/S0022143000029804

Christie, F. D. W., Steig, E. J., Gourmelen, N., Tett, S. F. B., & Bingham, R. G. (2023). Inter-decadal climate variability induces differential ice response along Pacific-facing West Antarctica. *Nature Communications*, *14*(93), 93. https://doi.org/10.1038/s41467-022-35471-3

Cornford, S. L., Seroussi, H., Asay-Davis, X. S., Gudmundsson, G. H., Arthern, R., Borstad, C., et al. (2020). Results of the third Marine Ice Sheet Model Intercomparison Project (MISMIP+). *The Cryosphere*, *14*(7), 2283–2301. https://doi.org/10.5194/tc-14-2283-2020

Cuffey, K. M., & Kavanaugh, J. L. (2011). How nonlinear is the creep deformation of polar ice? A new field assessment. *Geology*, *39*(11), 1027–1030. https://doi.org/10.1130/G32259.1

Cuffey, K. M., & Paterson, W. S. B. (2010). *The physics of glaciers* (4th ed.). Butterworth-Heinemann.

Denton, G. H., Hughes, T. J., Fastook, J. L., Schilling, D. H., & Lingle, C. S. (1979). Reconstruction and disintegration of ice sheets for the CLIMAP 18,000 and 125,000 years B.P. experiments: Results. *Journal of Glaciology*, *24*(90), 495–496. https://doi.org/10.3189/S0022143000015069

Feldmann, J., & Levermann, A. (2015). Collapse of the West Antarctic Ice Sheet after local destabilization of the Amundsen Basin. *Proceedings of the National Academy of Sciences of the United States of America*, *112*(46), 14191–14196. https://doi.org/10.1073/pnas.1512482112

Gerrish, L., Fretwell, P., & Cooper, P. (2020). Medium resolution vector polygons of Antarctic rock outcrop (7.3) [Dataset]. *UK Polar Data Centre, Natural Environment Research Council, UK Research & Innovation*. https://doi.org/10.5285/077e1f04-7068-4327-a4f2-71d863f70064

Gerrish, L., Ireland, L., Fretwell, P., & Cooper, P. (2024). Medium resolution vector polylines of the Antarctic coastline (7.9) [Dataset]. *UK Polar Data Centre, Natural Environment Research Council, UK Research & Innovation*. https://doi.org/10.5285/f2792d06-1e9d-4e00-a5c6-37d43bee5297

Getraer, B. (2024). proj-n4 (1.0.0) [Software]. *Zenodo*. https://doi.org/10.5281/zenodo.13750794

Gillet-Chaulet, F., Hindmarsh, R. C. A., Corr, H. F. J., King, E. C., & Jenkins, A. (2011). In-situ quantification of ice rheology and direct measurement of the Raymond Effect at Summit, Greenland using a phase-sensitive radar. *Geophysical Research Letters*, *38*(24), L24503. https://doi.org/10.1029/2011GL049843

Glen, J. W. (1952). Experiments on the deformation of ice. *Journal of Glaciology*, *2*(12), 111–114. https://doi.org/10.3189/S0022143000034067

Goelzer, H., Nowicki, S., Payne, A., Larour, E., Seroussi, H., Lipscomb, W. H., et al. (2020). The future sea-level contribution of the Greenland Ice Sheet: A multi-model ensemble study of ISMIP6. *The Cryosphere*, *14*(9), 3071–3096. https://doi.org/10.5194/tc-14-3071-2020

Goldsby, D. L., & Kohlstedt, D. L. (2001). Superplastic deformation of ice: Experimental observations. *Journal of Geophysical Research*, *106*(B6), 11017–11030. https://doi.org/10.1029/2000JB900336

Hughes, T. J. R., Liu, W. K., & Zimmermann, T. K. (1981). Lagrangian-Eulerian finite-element formulation for incompressible viscous flows. *Computer Methods in Applied Mechanics and Engineering*, *29*(3), 329–349. https://doi.org/10.1016/0045-7825(81)90049-9

ISSM Team. (2024). Ice-sheet and Sea-level System Model – ISSM [Software]. *California Institute of Technology*. Retrieved from https://github.com/ISSMteam/ISSM

Jezek, K. C., Alley, R. B., & Thomas, R. H. (1985). Rheology of glacier ice. *Science*, *227*(4692), 1335–1337. https://doi.org/10.1126/science.227.4692.1335

Jourdain, N. C., Asay-Davis, X., Hattermann, T., Straneo, F., Seroussi, H., Little, C. M., & Nowicki, S. (2020). A protocol for calculating basal melt rates in the ISMIP6 Antarctic Ice Sheet projections. *The Cryosphere*, *14*(9), 3111–3134. https://doi.org/10.5194/tc-14-3111-2020

Larour, E., Seroussi, H., Morlighem, M., & Rignot, E. (2012). Continental scale, high order, high spatial resolution, ice sheet modeling using the Ice Sheet System Model (ISSM). *Journal of Geophysical Research*, *117*(F1), F01022. https://doi.org/10.1029/2011JF002140

MacAyeal, D. R. (1989). Large-scale ice flow over a viscous basal sediment: Theory and application to Ice Stream B, Antarctica. *Journal of Geophysical Research*, *94*(B4), 4071–4087. https://doi.org/10.1029/JB094iB04p04071

Martín, C., Hindmarsh, R. C. A., & Navarro, F. J. (2006). Dating ice flow change near the flow divide at Roosevelt Island, Antarctica, by using a thermomechanical model to predict radar stratigraphy. *Journal of Geophysical Research*, *111*(F1), F01011. https://doi.org/10.1029/2005JF000326

Milillo, P., Rignot, E., Rizzoli, P., Scheuchl, B., Mouginot, J., Bueso-Bello, J., & Prats-Iraola, P. (2019). Heterogeneous retreat and ice melt of Thwaites Glacier, West Antarctica. *Science Advances*, *5*(1). https://doi.org/10.1126/sciadv.aau3433

Millstein, J. D., Minchew, B. M., & Pegler, S. S. (2022). Ice viscosity is more sensitive to stress than commonly assumed. *Communications Earth & Environment*, *3*(57), 57. https://doi.org/10.1038/s43247-022-00385-x

Minchew, B. M., Meyer, C. R., Robel, A. A., Gudmundsson, G. H., & Simons, M. (2018). Processes controlling the downstream evolution of ice rheology in glacier shear margins: Case study on Rutford Ice Stream, West Antarctica. *Journal of Glaciology*, *64*(246), 583–594. https://doi.org/10.1017/jog.2018.47

Montagnat, M., & Duval, P. (2004). The viscoplastic behaviour of ice in polar ice sheets: Experimental results and modelling. *Comptes Rendus Physique*, *5*(7), 699–708. https://doi.org/10.1016/j.crhy.2004.06.002

Morlighem, M. (2022). MEaSUREs BedMachine Antarctica (NSIDC-0756, Version 3) [Dataset]. *NASA National Snow and Ice Data Center Distributed Active Archive Center*. https://doi.org/10.5067/FPSU0V1MWUB6

Morlighem, M., Goldberg, D., Dias dos Santos, T., Lee, J., & Sagebaum, M. (2021). Mapping the sensitivity of the Amundsen Sea Embayment to changes in external forcings using automatic differentiation. *Geophysical Research Letters*, *48*(23), e2021GL095440. https://doi.org/10.1029/2021GL095440

Morlighem, M., Rignot, E., Binder, T., Blankenship, D., Drews, R., Eagles, G., et al. (2020). Deep glacial troughs and stabilizing ridges unveiled beneath the margins of the Antarctic Ice Sheet. *Nature Geoscience*, *13*(2), 132–137. https://doi.org/10.1038/s41561-019-0510-8

Morlighem, M., Seroussi, H., Larour, E., & Rignot, E. (2013). Inversion of basal friction in Antarctica using exact and incomplete adjoints of a higher-order model. *Journal of Geophysical Research: Earth Surface*, *118*(3), 1746–1753. https://doi.org/10.1002/jgrf.20125

Mouginot, J., Rignot, E., Scheuchl, B., & Millan, R. (2017). Comprehensive annual ice sheet velocity mapping using Landsat-8, Sentinel-1, and RADARSAT-2 data. *Remote Sensing*, *9*(4), 364. https://doi.org/10.3390/rs9040364

Nowicki, S., Goelzer, H., Seroussi, H., Payne, A. J., Lipscomb, W. H., Abe-Ouchi, A., et al. (2020). Experimental protocol for sea level projections from ISMIP6 stand-alone ice sheet models. *The Cryosphere*, *14*(7), 2331–2368. https://doi.org/10.5194/tc-14-2331-2020

Nowicki, S., Simon, E., & ISMIP6 Team. (2021). ISMIP6 21st century forcing datasets [Dataset]. The *Ghub*. https://doi.org/10.5281/zenodo.11176009

Nye, J. F. (1953). The flow law of ice from measurements in glacier tunnels, laboratory experiments and the Jungfraufirn borehole experiment. *Proceedings of the Royal Society of London. Series A. Mathematical and Physical Sciences*, *219*(1193), 477–489. https://doi.org/10.1098/rspa.1953.0161

Nye, J. F. (1957). *Physical properties of crystals: Their representation by tensors and matrices*. Oxford University Press.

Paterson, W. S. B., & Savage, J. C. (1963). Measurements on Athabasca Glacier relating to the flow law of ice. *Journal of Geophysical Research*, *68*(15), 4537–4543. https://doi.org/10.1029/JZ068i015p04537

Pattyn, F., & Morlighem, M. (2020). The uncertain future of the Antarctic Ice Sheet. *Science*, *367*(6484), 1331–1335. https://doi.org/10.1126/science.aaz5487

Pattyn, F., Perichon, L., Aschwanden, A., Breuer, B., de Smedt, B., Gagliardini, O., et al. (2008). Benchmark experiments for higher-order and full-Stokes ice sheet models (ISMIP-HOM). *The Cryosphere*, *2*(2), 95–108. https://doi.org/10.5194/tc-2-95-2008

Qi, C., Goldsby, D. L., & Prior, D. J. (2017). The down-stress transition from cluster to cone fabrics in experimentally deformed ice. *Earth and Planetary Science Letters*, *471*, 136–147. https://doi.org/10.1016/j.epsl.2017.05.008

Ranganathan, M., & Minchew, B. (2024). A modified viscous flow law for natural glacier ice: Scaling from laboratories to ice sheets. *Proceedings of the National Academy of Sciences of the United States of America*, *121*(23), e2309788121. https://doi.org/10.1073/pnas.2309788121

Raymond, C. F. (1973). Inversion of flow measurements for stress and rheological parameters in a valley glacier. *Journal of Glaciology*, *12*(64), 19–44. https://doi.org/10.3189/S0022143000022681

Rignot, E., Ciracì, E., Scheuchl, B., Tolpekin, V., Wollersheim, M., & Dow, C. (2024). Widespread seawater intrusions beneath the grounded ice of Thwaites Glacier, West Antarctica. *Proceedings of the National Academy of Sciences of the United States of America*, *121*(22), e2404766121. https://doi.org/10.1073/pnas.2404766121

Rignot, E., Mouginot, J., & Scheuchl, B. (2017). MEaSUREs InSAR-based Antarctica ice velocity map (NSIDC-0484, Version 2) [Dataset]. *NASA National Snow and Ice Data Center Distributed Active Archive Center*. https://doi.org/10.5067/D7GK8F5J8M8R

Rignot, E., Mouginot, J., Scheuchl, B., van den Broeke, M., van Wessem, M. J., & Morlighem, M. (2019). Four decades of Antarctic Ice Sheet mass balance from 1979–2017. *Proceedings of the National Academy of Sciences of the United States of America*, *116*(4), 1095–1103. https://doi.org/10.1073/pnas.1812883116

Scambos, T. A., Bell, R. E., Alley, R. B., Anandakrishnan, S., Bromwich, D. H., Brunt, K., et al. (2017). How much, how fast?: A science review and outlook for research on the instability of Antarctica's Thwaites Glacier in the 21st century. *Global and Planetary Change*, *153*, 16–34. https://doi.org/10.1016/j.gloplacha.2017.04.008

Schoof, C. (2012). Marine ice sheet stability. *Journal of Fluid Mechanics*, *698*, 62–72. https://doi.org/10.1017/jfm.2012.43

Schwans, E., Parizek, B. R., Alley, R. B., Anandakrishnan, S., & Morlighem, M. (2023). Model insights into bed control on retreat of Thwaites Glacier, West Antarctica. *Journal of Glaciology*, *69*(277), 1241–1259. https://doi.org/10.1017/jog.2023.13

Seroussi, H., Morlighem, M., Larour, E., Rignot, E., & Khazendar, A. (2014). Hydrostatic grounding line parameterization in ice sheet models. *The Cryosphere*, *8*(6), 2075–2087. https://doi.org/10.5194/tc-8-2075-2014

Seroussi, H., Nakayama, Y., Larour, E., Menemenlis, D., Morlighem, M., Rignot, E., & Khazendar, A. (2017). Continued retreat of Thwaites Glacier, West Antarctica, controlled by bed topography and ocean circulation. *Geophysical Research Letters*, *44*(12), 6191–6199. https://doi.org/10.1002/2017GL072910

Seroussi, H., Nowicki, S., Payne, A. J., Goelzer, H., Lipscomb, W. H., Abe-Ouchi, A., et al. (2020). ISMIP6 Antarctica: A multi-model ensemble of the Antarctic Ice Sheet evolution over the 21st century. *The Cryosphere*, *14*(9), 3033–3070. https://doi.org/10.5194/tc-14-3033-2020

Summers, P. T., Elsworth, C. W., Dow, C. F., & Suckale, J. (2023). Migration of the shear margins at Thwaites Glacier: Dependence on basal conditions and testability against field data. *Journal of Geophysical Research: Earth Surface*, *128*(3), e2022JF006958. https://doi.org/10.1029/2022JF006958

Thomas, R. H. (1973). The creep of ice shelves: Interpretation of observed behaviour. *Journal of Glaciology*, *12*(64), 55–70. https://doi.org/10.3189/S002214300002270X

Thomas, R. H. (1979). The dynamics of marine ice sheets. *Journal of Glaciology*, *24*(90), 167–177. https://doi.org/10.3189/S0022143000014726

Thomas, R. H., & Bentley, C. R. (1978). A model for holocene retreat of the West Antarctic Ice Sheet. *Quaternary Research*, *10*(2), 150–170. https://doi.org/10.1016/0033-5894(78)90098-4

Thomas, R. H., MacAyeal, D. R., Bentley, C. R., & Clapp, J. L. (1980). The creep of ice, geothermal heat flow, and Roosevelt Island, Antarctica. *Journal of Glaciology*, *25*(91), 47–60. https://doi.org/10.3189/S0022143000010273

Weertman, J. (1974). Stability of the junction of an ice sheet and an ice shelf. *Journal of Glaciology*, *13*(67), 3–11. https://doi.org/10.3189/S0022143000023327

Weertman, J. (1983). Creep deformation of ice. *Annual Review of Earth and Planetary Sciences*, *11*(1), 215–240. https://doi.org/10.1146/annurev.ea.11.050183.001243

Zeitz, M., Levermann, A., & Winkelmann, R. (2020). Sensitivity of ice loss to uncertainty in flow law parameters in an idealized one-dimensional geometry. *The Cryosphere*, *14*(10), 3537–3550. https://doi.org/10.5194/tc-14-3537-2020